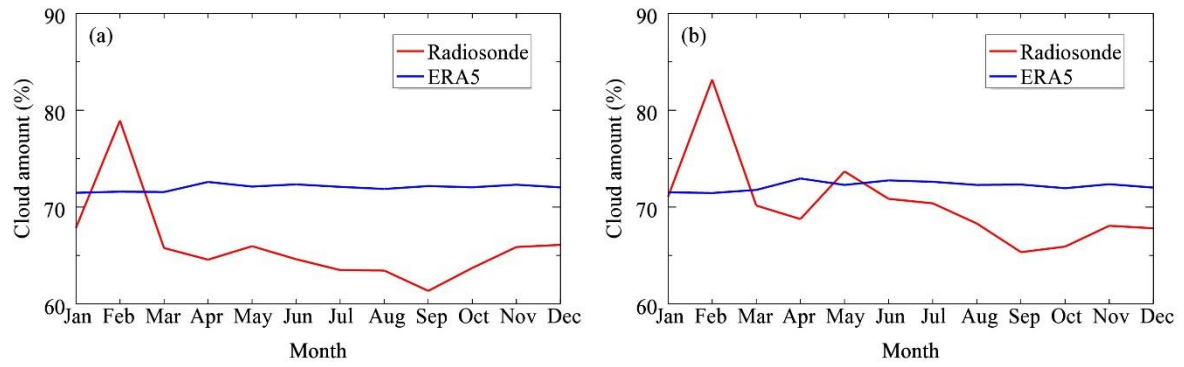


1

**FIGURES**

2

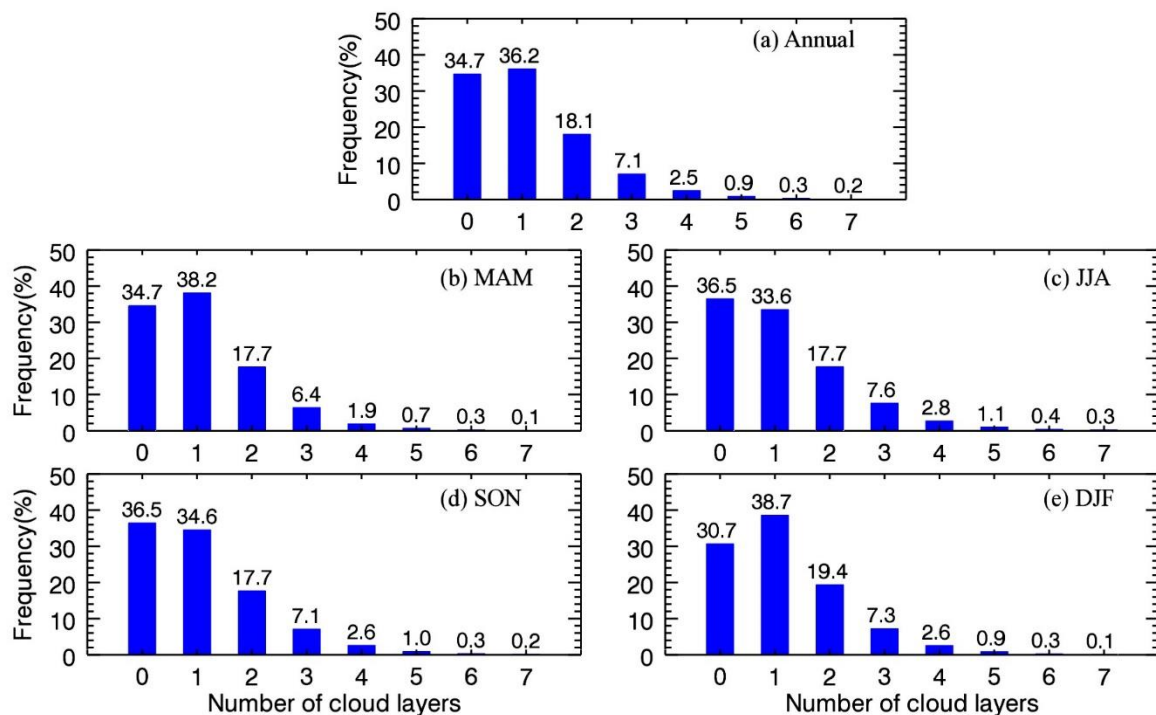


3

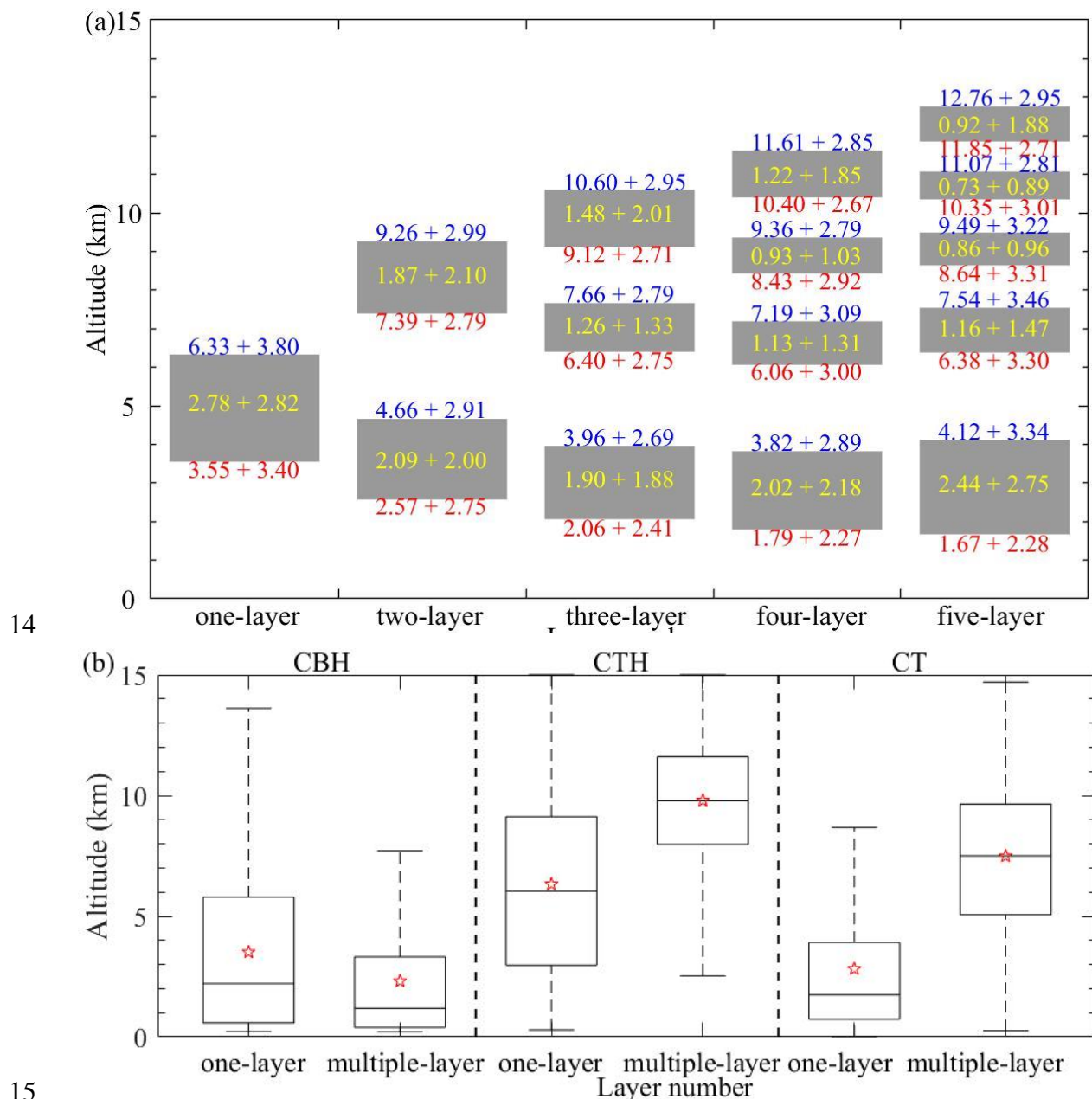
4 **Figure S1.** The monthly cloud amount at (a) 0000 UTC, and (b) 1200 UTC. The red and blue

5 lines represent the cloud amount from radiosonde and ERA5, respectively.

6

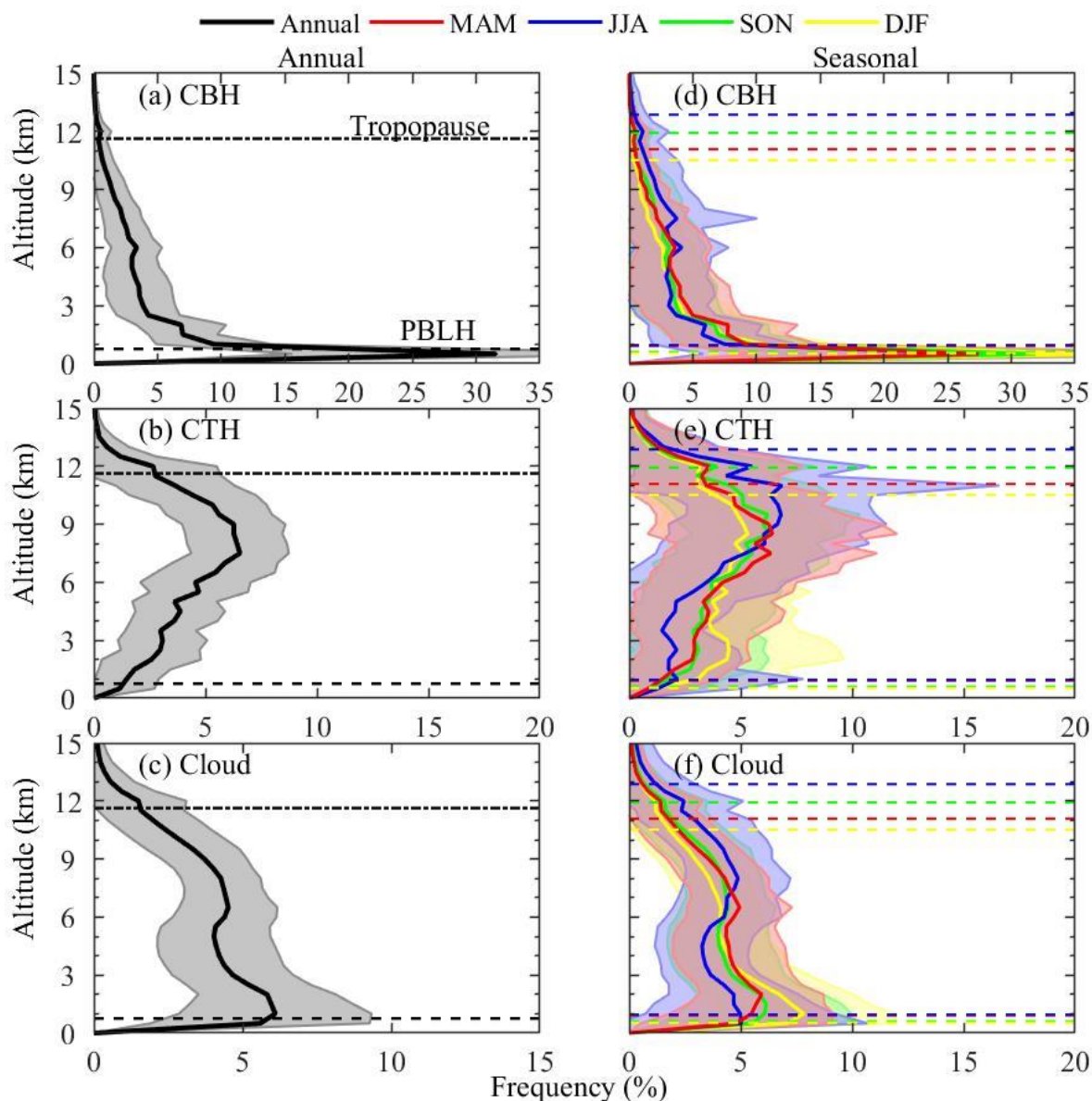


7  
8 **Figure S2.** Near-global mean occurrence frequencies of clouds with a variety of layers  
9 ranging from 0 to 7 as detected by high-resolution radiosonde measurements at 0000 UTC  
10 during the period of 2018–2019: (a) annual, (b) March–April–May (MAM), (c) June–July–  
11 August (JJA), (d) September–October–November (SON), and (e) December–January–  
12 February (DJF). Also marked is the probability for the specified cloud type at the top of each  
13 bar.

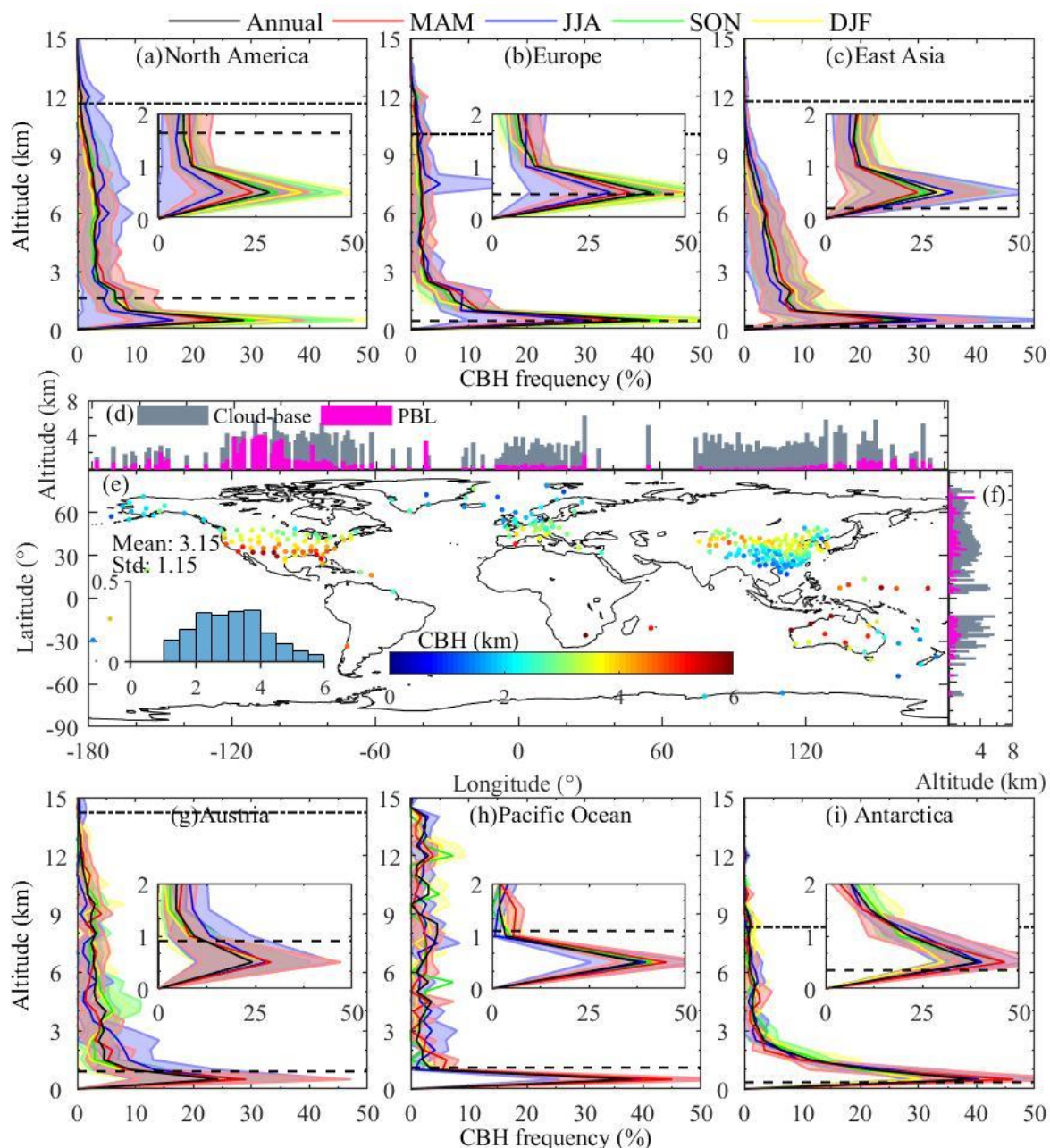


15  
 16 **Figure S3.** Near-global annual mean (a) vertical locations of one-, two-, three-, four-, and  
 17 five-layer clouds and (b) boxplot of CVS (CBH, CTH, and CT) for one- and multi-layer  
 18 clouds at 0000 UTC during the period of 2018–2019. The mean  $\pm$  one standard deviation  
 19 values of CBH, CTH, and CT for each cloud type are also marked in (a).

20

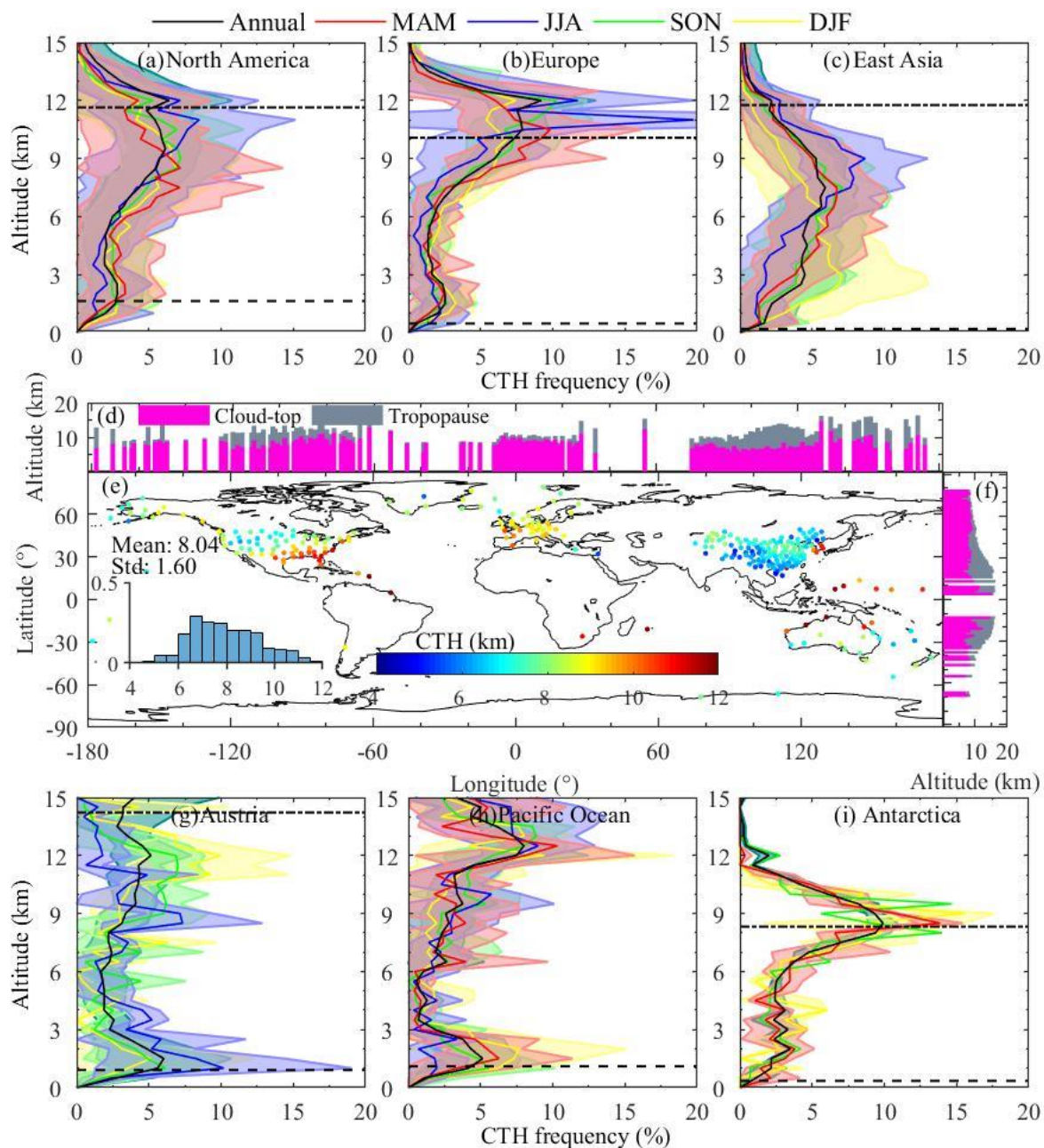


21  
 22 **Figure S4.** Near-global mean vertical distributions of (a-c) annual and (d-f) seasonal  
 23 occurrence frequencies of CBHs, CTHs, and clouds as detected by radiosonde data at 0000  
 24 UTC during the period of 2018–2019, respectively. The annual, MAM, JJA, SON, and DJF  
 25 are marked in black, red, blue, green, and yellow, respectively. Samples are vertically divided  
 26 with a resolution of 500 m. The percentage for a given altitude is defined as the ratio of  
 27 cloudy samples on that altitude to all cloudy samples. The solid lines are the mean values and  
 28 shadows are the one standard deviation at annual or a given season. The planetary boundary  
 29 layer height (PBLH) is determined with the method proposed by Vogelezang and Holtslag  
 30 (1996), marked in dot-hyphen, and the tropopause is defined with the method from WMO  
 31 (1957), marked in hyphen. The determination of PBLH and tropopause are detailed in the  
 32 Supplementary Information.



33

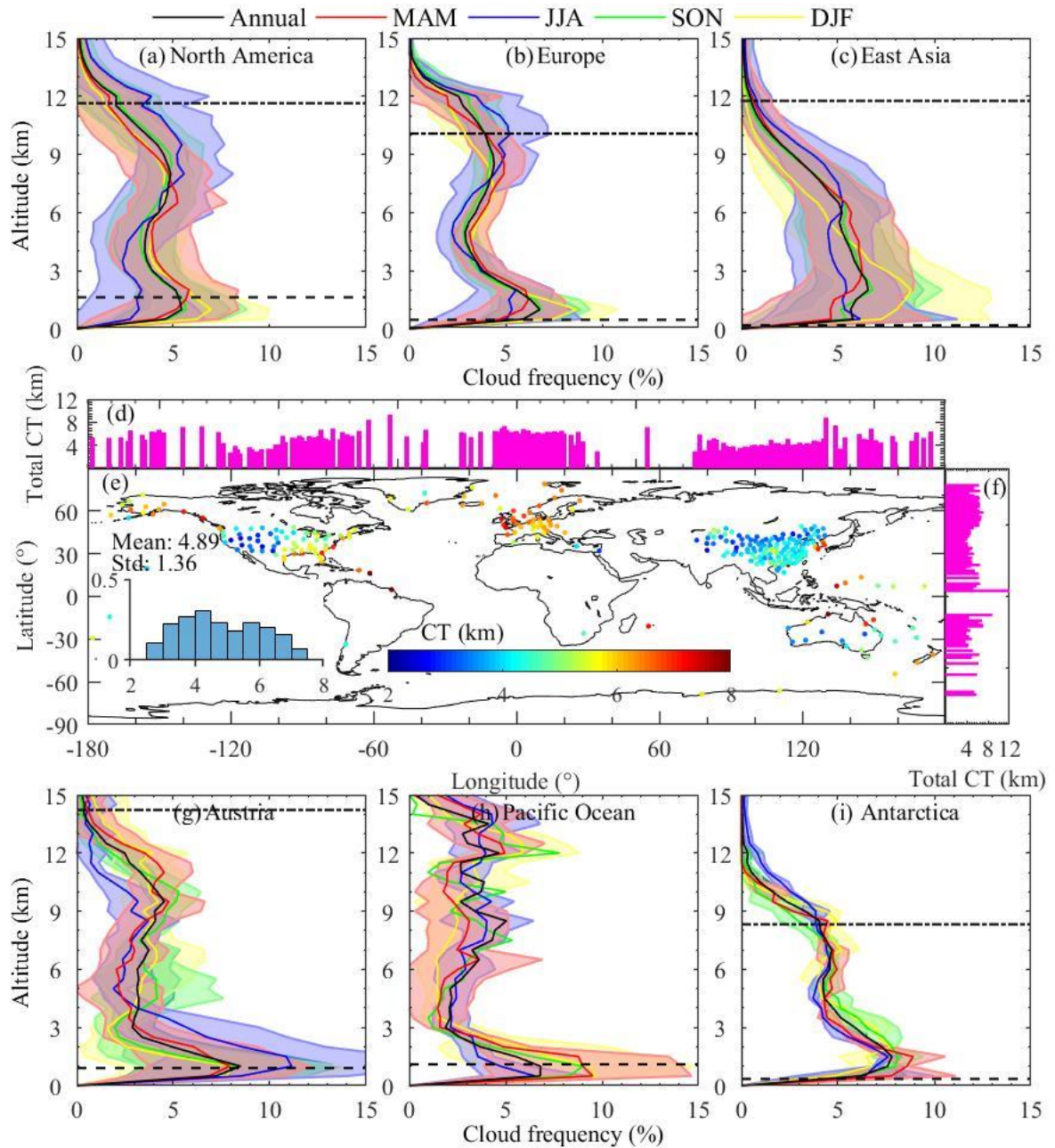
34 **Figure S5.** Regional mean vertical distributions of the occurrence frequencies of CBHs at  
 35 0000 UTC during the period of 2018–2019. The altitude resolved annual and seasonal  
 36 averaged occurrence frequencies of CBHs are displayed in (a-c, g-i) over six regions of  
 37 interest, including North America, Europe, East Asia, Austria, Pacific Ocean, Polar. Also  
 38 shown are the near-global geographic distribution of the annual mean CBH (e), with the  
 39 histogram of the probability distribution for CBH in the inset and the corresponding  
 40 meridional (d) and zonal (f) means overlaid with the mean PBLH.



41

42 **Figure S6.** Similar as Figure 5, but for the occurrence frequencies of CTHs at 0000 UTC  
 43 during the period of 2018–2019.

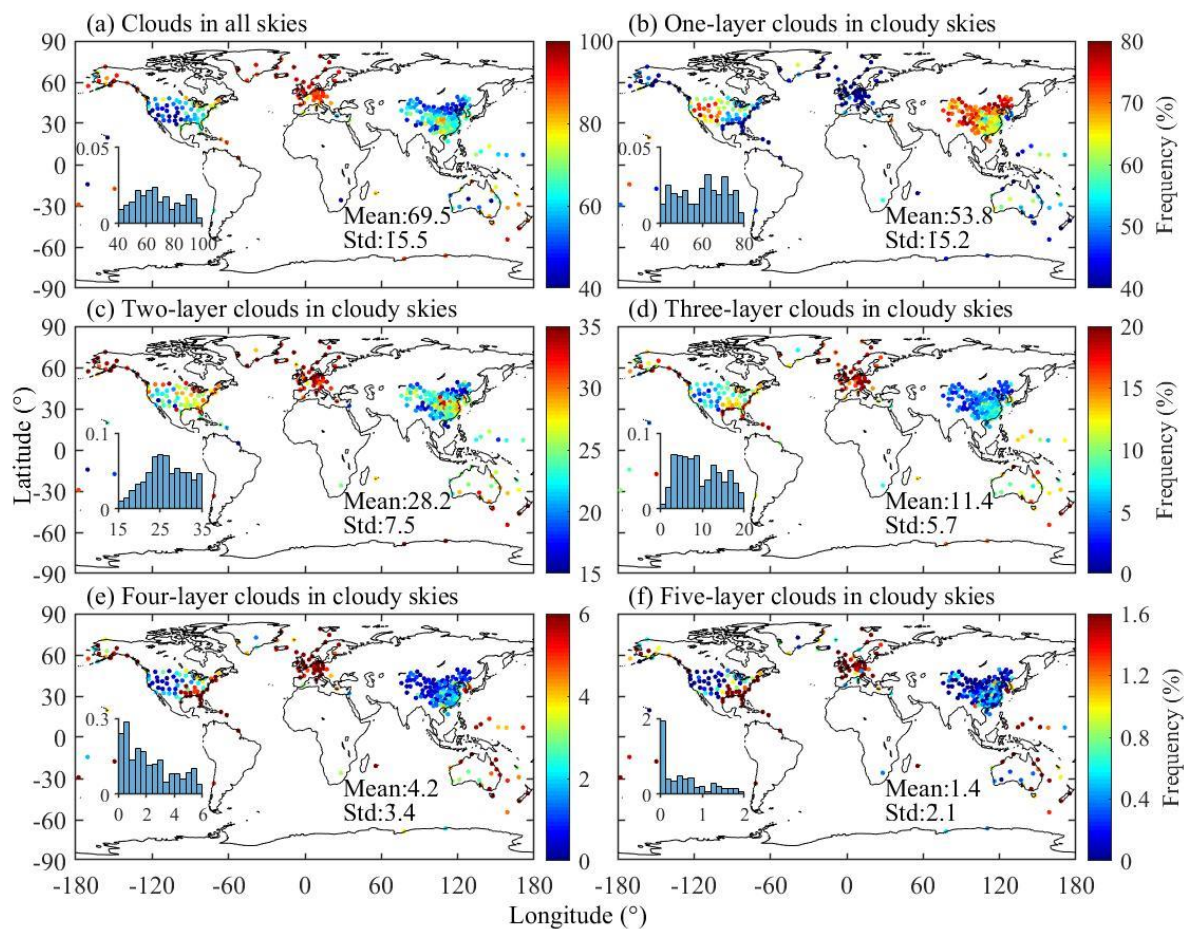
44



45

46 **Figure S7.** Similar as Figure S5, but for the occurrence frequencies of clouds at 0000 UTC  
 47 during the period of 2018–2019.

48

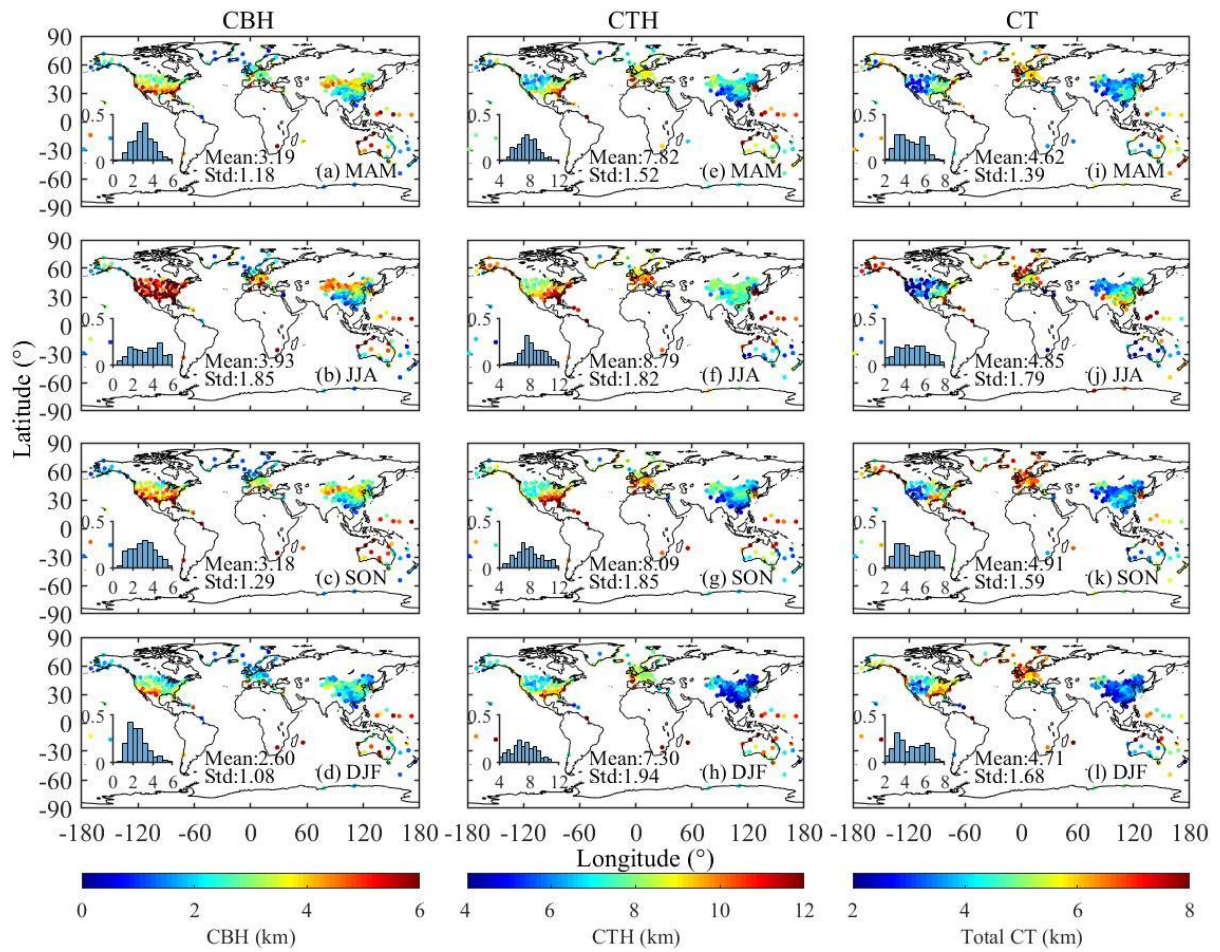


49

50 **Figure S8.** The geographic distributions of the occurrence frequencies of (a) clouds in all  
 51 skies, and (b–f) one-, two-, three-, four-, and five-layer clouds in cloudy skies at 0000 UTC  
 52 during the period of 2018–2019. It should be noted that the range of the colorbar differ a lot  
 53 in order to improve the visual interpretation. Also shown are the histograms of probability  
 54 distributions for the cloud occurrence frequencies in each panel.

55

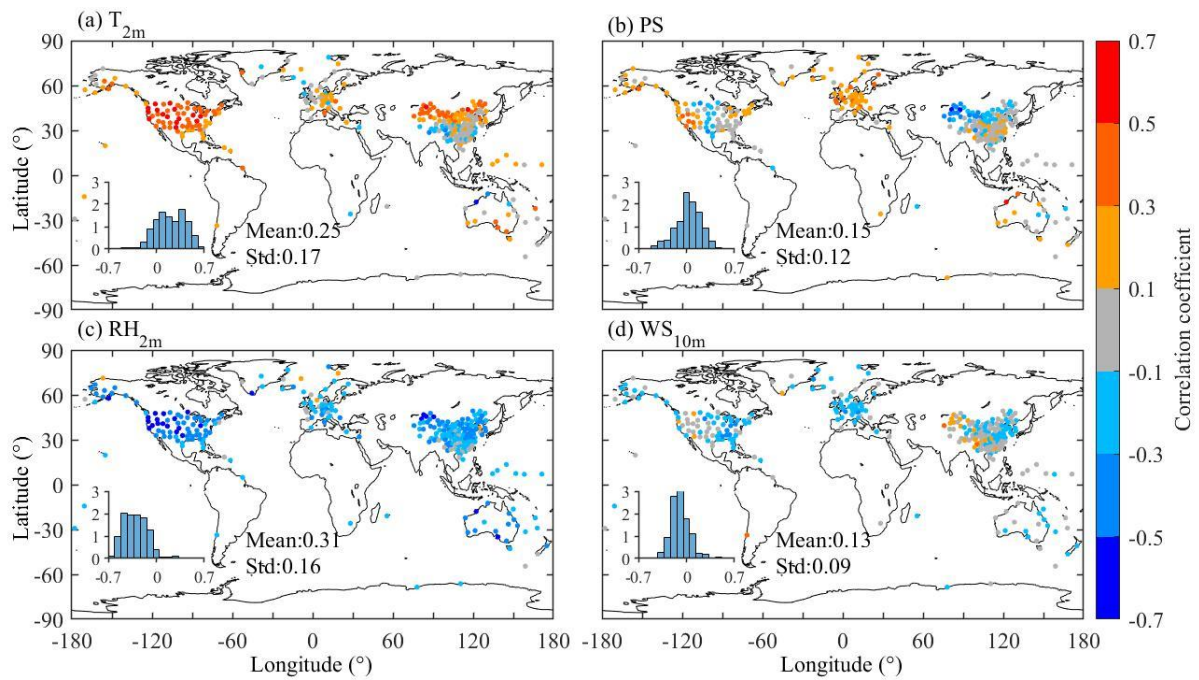




56

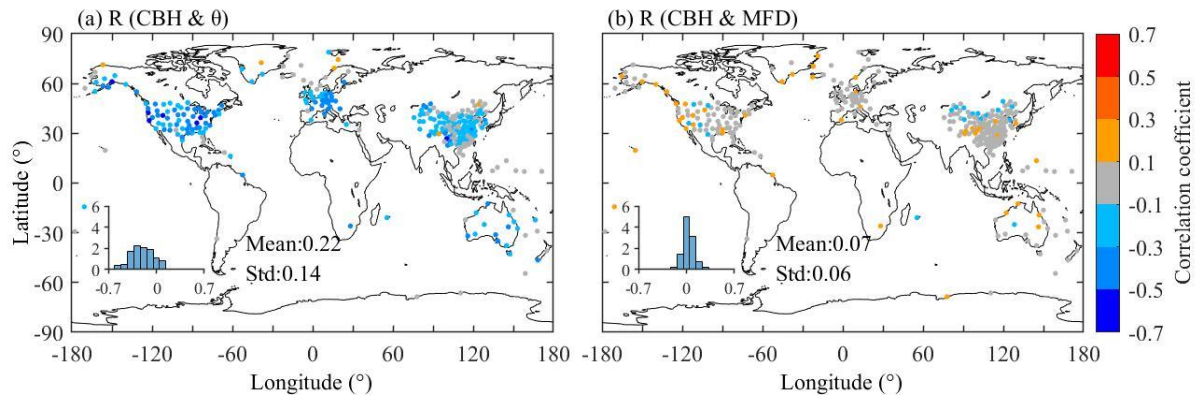
57 **Figure S9.** The geographic distributions of the seasonal mean CBHs (a-d), CTHs (e-h), and  
 58 CTs (i-l) at 0000 UTC during the period of 2018–2019. Also shown are the histograms of  
 59 probability distributions for the CVS in each panel.

60



61  
 62 **Figure S10.** Geographic distributions of the correlation coefficients ( $R$ ) between radiosonde-  
 63 derived CBH and surface meteorological variables: (a) 2m air temperature ( $T_{2m}$ ), (b) surface  
 64 pressure (PS), (c) 2m relatively humidity ( $RH_{2m}$ ), and (d) 10m wind speed ( $WS_{10m}$ ) at 0000  
 65 UTC during the period of 2018–2019. Also shown are the histograms of probability  
 66 distributions for their corresponding  $R$  values in each panel.

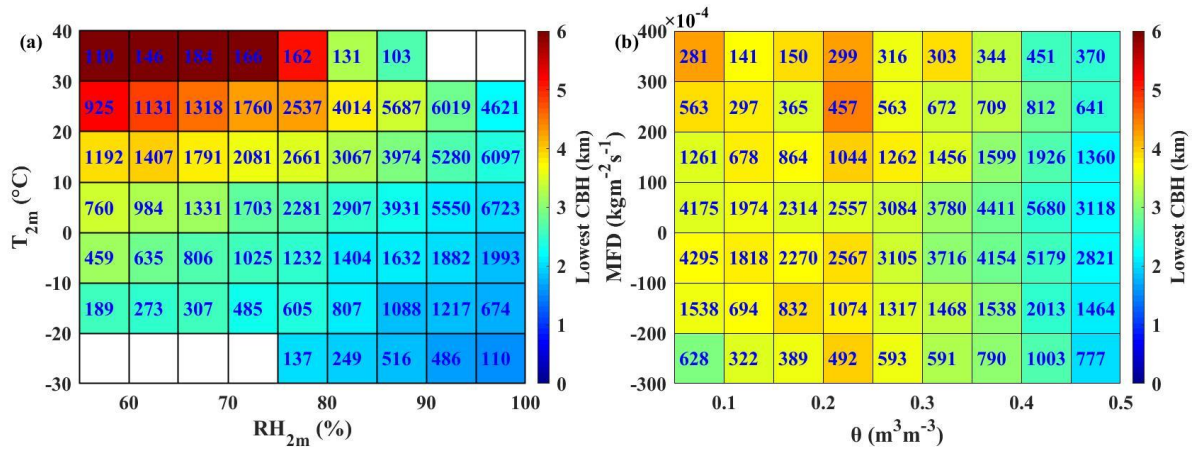
67



68

69 **Figure S11.** The same as Figure 14, but for the correlations between CBH and (a) soil water  
70 content ( $\theta$ ) and (b) moist flux divergence (MFD) at 0000 UTC during the period of 2018–  
71 2019.

72



73

74 **Figure S12.** Joint dependences of CBH on (a)  $T_{2m}$  and  $RH_{2m}$ , (b)  $\theta$  and MFD at 0000

75 UTC during the period of 2018–2019. Note that the number labeled in each cell represents its

76 corresponding sample size.

77